International Journal of Mining Science and Technology xxx (xxxx) xxx

Contents lists available at ScienceDirect

International Journal of Mining Science and Technology

journal homepage: www.elsevier.com/locate/ijmst

An improved outer pipe method for expansive pressure measurement of static cracking agents

Shuai Xu [a], Pengyuan Hou [a], Runran Li [a], Fidelis T. Suorineni [a,b,*]

[a] Key Laboratory of Ministry of Education on Safe Mining of Deep Metal Mines, Northeastern University, Shenyang 110819, China
[b] School of Mining and Geosciences, Nazarbayev University, Astana 010000, Kazakhstan

ARTICLE INFO

Article history:
Received 5 February 2020
Received in revised form 13 September 2020
Accepted 30 November 2021
Available online xxxx

Keywords:
Static cracking agent
Hydration reaction
Expansive pressure measurement
Outer pipe method
Upper end surface method, Numerical simulation

ABSTRACT

Static cracking agent (SCA) is actively investigated as an alternative to explosive blasting for rock breakage due to its immense expansion property. SCA can eliminate the negative effects of shock, noise and harmful gases encountered in explosive blasting processes. Accurate measurement and deep understanding of the expansive properties of SCAs are important in their industrial application. An improved outer pipe method (OPM), termed the upper end surface method (UESM), is proposed in this paper to overcome the shortcomings of the OPM in the expansive pressure measurement of SCAs. Numerical simulation is used to proof the concept and a mathematical model established to relate the internal pressure and the radial strains at different positions in the upper end surface method test equipment. The new equipment is calibrated using oil pressure and strain measurements. The calibrated equipment is then used to measure the expansion pressure of SCA at three different water contents to proof its potential. The differences in the measurements with OPM and UESM at three different moisture contents are less than 4%. The experimental results confirm the accuracy and applicability of the more user friendly and less expensive UESM in the measurement of the expansive pressures of SCAs.

1. Introduction

Static cracking agent (SCA), is also known as soundless cracking agent [1], soundless chemical cracking agent [2], non-explosive cracking agent [3], non-explosive splitting compound [4], expansive cement [5], expansive chemical splitter [6], expansive demolition agent [7] or soundless cracking demolition agent (SCDA) [8]. In this paper, the name static cracking agent (SCA) is adapted. SCA is a high expansion powdered cementitious material that can replace explosive blasting in rock fragmentation. Compared with explosive blasting, the hydration reaction of SCA is relatively slow, the expansive pressure generated by the reaction applies uniformly to the rock mass, and no shock, noise or flying rock (which is common in explosive blasting) is experienced in the expansion process [6,9] and fragmentation of the rock mass. Therefore, SCA has been widely applied to stone quarrying [10], rock mass breakage [3,11,12] in excavations, shale gas extraction [13,14], rock mass fracturing in heap leaching mining [15], rockmass support [16,17] and in rock engineering for discontinuity persistence and tensile strength studies [6,18].

The main component of SCA is dead-burn calcium oxide (CaO) [19]. A gelatinous $Ca(OH)_2$ which is formed after CaO reaction with water crystallizes continuously. The crystals separate out from the saturated solution, resulting in continuous generation of $Ca(OH)_2$. The newly formed products keep accumulating on the previous products, which results in the expansion of the reaction products [20]. The $Ca(OH)_2$ crystals generated by the hydration reaction dilate and invade the space previously occupied by the CaO reducing the voids between the CaO crystals. The relatively small pores between the crystals further enhances the volume expansion, and the generation of the crystals (products after the hydration reaction) of the SCA, leading to relatively large expansive pressure [18-23]. The expansive pressure of SCA results from the combined effects of the solid expansion and the porosity change in the hydration process [7,21].

Understanding the expansive pressure generation of SCA is of great significance to the industrial application of SCA [22-27]. Both temperature and water content have influence on the development of the expansive pressure [2,7] in SCA. A higher temperature leads to a faster hydration reaction, and more rapid increase of the expansive pressure. Previous studies on the hydration reaction of

* Corresponding author at: Key Laboratory of Ministry of Education on Safe Mining of Deep Metal Mines, Northeastern University, Shenyang 110819, China.
E-mail address: fidelis.suorineni@nu.edu.kz (F.T. Suorineni).

https://doi.org/10.1016/j.ijmst.2021.11.011
2095-2686/

SCA at intermediate or low temperatures showed that the expansive pressure changes linearly with the reaction time, and that SCA can expand 1.1 to 1.4 times more after the hydration reaction [25]. The 'pressure-time' curves of SCA in the hydration reaction process can be derived from the expansive pressure measurement tests on SCA at different water contents, which provides a theoretical basis for the industrial application of SCA [8,22,26].

Several methods have been commonly used to measure the expansive pressure of SCA, including the outer pipe method [7,21], the inner pipe method and the pressure sensor method [7].

In the outer pipe method (OPM) [7] (Fig. 1), the test device is a thick-walled cylindrical steel pipe with one closed end to prevent outflow of the SCA slurry. The theoretical basis of the OPM is therefore the thick-walled cylinder theory [7,27] in elastic mechanics. According to the theory of thick-walled cylinders with one end closed [7,28,29], based on the theory of elasticity, the pipe will deform when subjected to uniform internal pressure (P_r), and a mathematical relation between the deformation and the applied internal pressure can be determined (Eq. (1)) [7]. Eq. (1) is the theoretical basis for the calculation of the expansion pressure of SCA by OPM. The wall stress (Eq. (2) at the outer pipe surface at point Q in Fig. 2 can be determined according to the governing equations in [7,28,29]. Fig. 2 is a schematic representation of uniformly applied internal pressure on a thick-walled cylindrical pipe and shows the geometrical characteristics of the cylinder and strain measurement position at point Q.

$$P_r = \frac{E(k^2-1)}{2(1-v^2)}(\varepsilon_\phi + v\varepsilon_z) \tag{1}$$

where E is elastic modulus of steel; v Poisson's ratio; k the ratio of the outer radius to the inner radius of the steel pipe; ε_ϕ the circumferential strain; and ε_z the axial strain at the outer pipe wall.

Eqs. (3) and (4) define the tangential (ε_ϕ) and axial (ε_z) strains in Eq. (1) based on the generalized Hooke's law, respectively.

$$\sigma_\phi = \frac{P_r a^2}{b^2-a^2}\left(1+\frac{b^2}{\rho^2}\right) \tag{2}$$

$$\varepsilon_\phi = \frac{1}{E}(\sigma_\phi - v\sigma_Z) \tag{3}$$

$$\varepsilon_z = \frac{1}{E}(\sigma_z - v\sigma_\phi) \tag{4}$$

From Eqs. (2)–(4), the internal pressure from SCA expansion can be determined from Eq. (1), knowing the strains ε_ϕ and ε_z at the outer wall of the cylinder where $\rho = b$ (i.e. point Q in Fig. 2.)

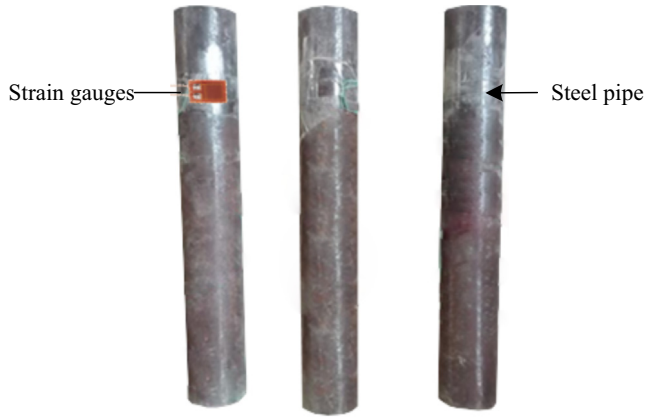

Fig. 1. Equipment for the outside pipe method with strain gauges on the outer surface of the 301 stainless steel pipe.

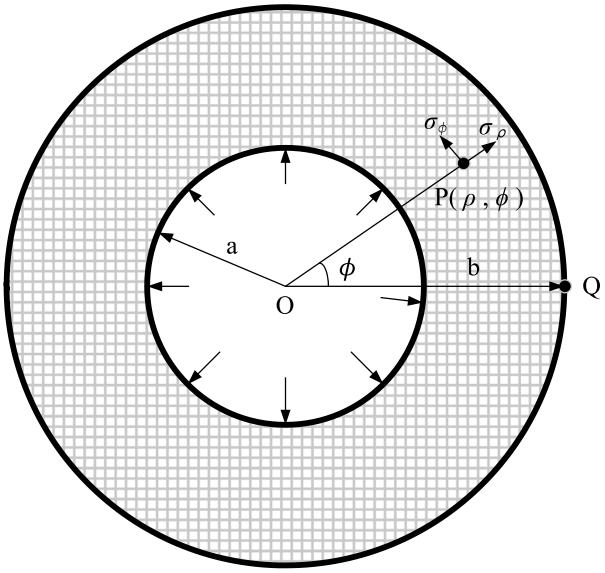

Fig. 2. Schematic representation of uniformly applied internal pressure on a thick-walled cylindrical pipe showing the geometrical characteristics of the cylinder and strain measurement position at point Q.

In practice, strain gauges are attached to the outer wall of the steel pipe so that when the steel pipe deforms due to the expansive pressure induced by the hydration reaction of SCA, the strain gauges measure the radial and tangential or circumferential strains, and Eq. (1) is used to calculate the expansive pressure of the SCA.

To avoid the temperature issues and other related problems with the OPM method, Harada et al. [7] developed the inner pipe method (IPM) to calculate the expansive pressure of SCA based on the measurement of the radial and tangential strains of the inner pipe (Eq. (5)) outer wall.

$$P_{ri} = \frac{E_s(k^2-1)}{2(1-v_s^2)}(\varepsilon_\phi + v_s\varepsilon_z) \tag{5}$$

where P_{ri} is the expansion pressure of SCA in the inner pipe method (IPM); and E_s and v_s the Young's modulus and Poisson's ratio of the steel, respectively.

In IPM, the strain gauges must be carefully attached to the inner pipe outer wall and the pipe placed in a concrete cylinder and the annulus between the steep pipe and concrete cylinder filled with the SCA slurry. This approach results in a complex testing procedure and high cost.

The pressure sensor method uses pressure sensors that are protected by inert gases and hydraulic pressure to directly measure the expansive pressure of the SCA reaction process [7]. The test cost of the pressure sensor method is higher than that of the outer and inner pipe methods since the pressure sensor needs to be specially manufactured and handled.

2. The problem and objective

An expansive pressure calculation equation (Eq. (6)) developed by Gholinejad and Arshadnejad [30] is independent of the containing expansive material (e.g. cement, aluminum, plastics, and steel) behavior. This equation eliminates the influence of the pipe material on the expansive pressure test result and provides a new insight for research on expansive pressure testing of materials such as SCA.

$$P_r = 0.566 \times t^{0.933} \times d^{0.407} \times E^{0.493} \tag{6}$$

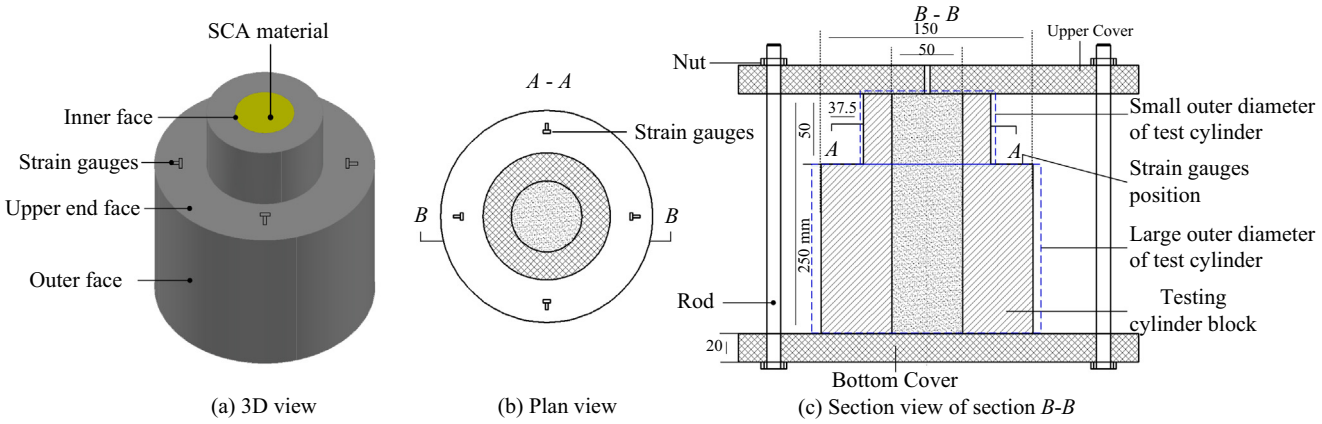

(a) 3D view (b) Plan view (c) Section view of section *B-B*

Fig. 3. Design drawing of the proposed SCA UESM expansive pressure measurement equipment. Numbers are dimensions in millimeters.

where t is time in hours of reaction; d the hole diameter of cylinder; and E Young's modulus of the cylinder material. The SCA used in developing Eq. (6) was of Iranian manufacture, with the trade name Katrock [30]. Also, only tangential strains were measured in the study. Other SCA types may not yield the same results and require a future study.

The accurate measurement of the expansive pressure of SCA is vital for its industrial performance evaluation, parameter selection and cost control. In this paper, an innovative SCA expansive pressure measurement method is proposed, termed the upper end surface method (UESM). This method overcomes the problems in the outer pipe and inner pipe methods.

When testing SCA expansion pressure with OPM, the material of the test device used is generally a stainless steel. In the Chinese standard for testing the expansion pressure with the OPM, it is required to place the OPM test device in an ice-water mixture to reduce the temperature. Laefer and Zolanvari [27] also used the same ice cooling methods with the OPM. Alternatively, to avoid the influence of high temperature on strain measurement, some researchers use 3D speckle devices instead of strain gauges to overcome the high temperature problem in the OPM to test SCA expansion pressure. However, speckle measurement is restricted by many factors. Apart from the high cost of 3D speckle test equipment, the test accuracy is limited by the speckle spraying accuracy on the outer surface of the device.

In the case of the proposed UESM, the test device is a thick-walled 7075 aluminum alloy cylinder. In that case the heat transfer path is longer and the material heat conductivity and diffusivity is higher compared to the 301stainless steel used in the OPM. Hence, the final heat transferred to the outer surface of the proposed test system is less, resulting in temperatures suitable for the use of standard strain gauges with no additional measures for cooling. This is explained in detail in Section 4.

In this paper, the UESM test equipment design is presented, and the test procedure described. The proposed SCA UESM is first numerically simulated as a proof of concept. The SCA UESM is calibrated, and its accuracy and applicability validated. The calibrated UESM is then used to test SCA expansivity at various water contents. A mathematical model is then developed that relates the SCA expansive pressure and the radial strains at different measurement points in the UESM. Finally, both the OPM and UESM are used to measure the expansive pressure of SCA, and the results compared. The results show that the new method of measuring the expansive pressure of SCA is more accurate. The proposed method is also more user friendly and less expensive compared to the OPM and IPM in current use.

3. Numerical simulation of expansion process of SCA based on the upper end surface method

3.1. Numerical model setup and boundary conditions

The numerical modelling software Flac3D [31] was used to simulate the SCA expansion pressure measurement with the UESM. The authors acknowledge that FLAC3D cannot capture the several hours taken by SCA to expand in actual applications. In the numerical simulation analysis of the SCA expansion pressure the intent is to establish a relationship between the SCA expansion pressure and the strain at the selected monitoring positions due to selected imposed uniformly distributed normal pressure on the inner surface of the test cylinder device. The series of selected pressures of between 10 and 100 MPa implicitly capture the SCA expansion pressure levels at certain times in its expansion process. In this way, relationships between the SCA expansion pressure and the strain was established. Hence, in the calibration verification of the test device only the consistency of the test results with the experimental results was examined, without explicitly considering the time dependent expansion of actual SCA.

The dimensions of the numerical model were based on the UESM designed equipment shown in Fig. 3. Details of the UESM test equipment design and materials are provided in Section 4 of this paper. Fig. 3a shows the test cylinder has two parts. The total height of the test cylinder is 250 mm, with an inner diameter of 50 mm. The outer diameter of the lower 200-mm height of the test cylinder is 150 mm with a wall thickness of 50 mm, and the top 50 mm height has an external diameter of 75 mm with a wall thickness of 12.5 mm. In the numerical model (Fig. 4) the node

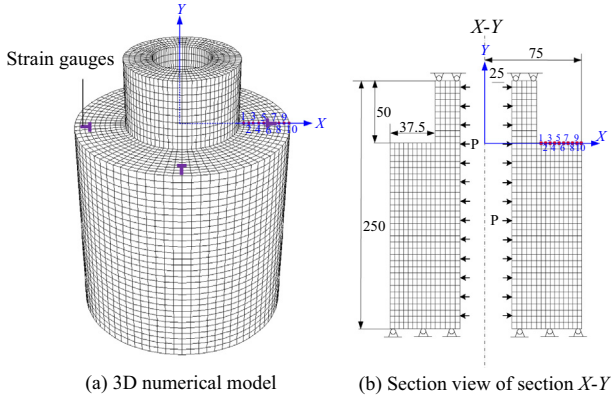

(a) 3D numerical model (b) Section view of section *X-Y*

Fig. 4. Setup of numerical simulation model showing strain monitoring points.

spacing is 5 mm in the vertical direction and 3.75 mm in the horizontal direction. The model has 32,800 elements and 36,800 nodes. The model is fixed in the top and bottom and only horizontal movement is allowed along the height of the test cylinder to allow for the expansion of the SCA. Selected normal stresses are applied to the inner wall of the test cylinder to simulate the expansion pressure of the SCA. Movement at the top and bottom of the test cylinder are restrained by the fixed top and bottom platens.

The displacements at the top and bottom boundaries are restricted in the numerical simulation. Surface forces are applied normal to the inner wall of the cylinder along its height as shown in Fig. 4.

3.2. Parameters in the numerical simulation

Linear elastic mechanics are adopted in the numerical simulation. The material parameters are listed in Table 1. In Table 1, manufacturers specifications of the properties of the 7075 Aluminum Alloy used in fabricating the UESM test device and those of the 301 stainless steel used in OPM test pipes are given. The reason for providing the properties of the stainless steel used in the OPM test device is to eventually explain any differences in the test results and benefits and limitations of the two test methods.

3.3. Strain monitoring

Ten strain monitoring points were arranged along the x-axis (i.e. the radial direction) at the top end surface of the 150-mm diameter section of the test cylinder as shown in Fig. 4. The strains are monitored at 10 locations labeled 1, 2, 3,...10 in the horizontal direction at distances of 42.5, 46.25, 50.0, 53.75, 57.5, 61.25, 65.0, 68.75, 72.5 and 76.25 mm respectively from the center of the test cylinder as shown in Fig. 4. The strain of the element in the numerical simulation (ε) is defined as the ratio between the displacement of the element and the original dimension of the element as given in Eq. (7):

$$\varepsilon = \frac{\Delta L}{L} \tag{7}$$

where ΔL is element change in displacement; and L the original length of the element along a given direction (axial or diametrical).

3.4. Numerical simulation schemes

In the numerical modelling, the SCA expansive pressure was increased from 10 to 100 MPa at 10 MPa intervals. The radial strain at each monitoring point at the upper end surface of the 150-mm diameter section of the test cylinder (Fig. 4) was recorded.

3.5. Strain variation ratio

Assuming the strains at two adjacent monitoring points are ε_n and ε_{n+1} respectively, the strain variation ratio defined in Eq. (8) represents the strain changing rate in the wall of the test cylinder for a given SCA expansive pressure in the numerical model.

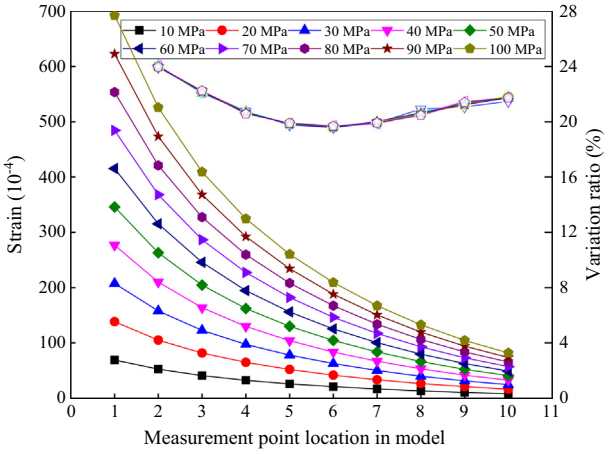

Fig. 5. Strain variations at the upper end surface at different expansive pressures.

$$\Delta\varepsilon = \frac{\varepsilon_n - \varepsilon_{n+1}}{\varepsilon_n} \tag{8}$$

The strain rate shows how fast the strain changes as the distance from the test cylinder center increases radially.

3.6. Analysis of numerical simulation results

3.6.1. Strains at each monitoring point at different expansive pressures

The strains at each monitoring point in Fig. 4 for given SCA expansive pressures are plotted in Fig. 5. The horizontal axis shows the monitoring points locations at different distances from the center of the test cylinder. The left vertical axis gives the strain values at the monitoring points, and the right vertical axis presents the strain variation ratio of two adjacent monitoring points. For a given SCA expansive pressure. The figure shows that the radial strain at each monitoring point decreases (as an exponential function) as the radial distance from the from the center of the test cylinder increases outwards.

In Fig. 5, the strain rate curve shows how fast the strain changes as the distance from the center of test cylinder increases. At a given strain monitoring point, the strain increases with increasing SCA expansive pressure. According to the strain variation ratio curve, the strain variation ratio decreases gradually from the center of the test cylinder outwards to a minimum and increases again. When the distance from the center of the test cylinder is about 61.25 mm, the strain variation ratio of the corresponding element reaches its minimum after which it increases again. The latter strain variation increments may be due to the influence of the model boundary as the strain monitoring points approached the outer edge of the model boundary.

3.6.2. Change of monitoring point strain against expansive pressure

The change of the strain value at a given monitoring point location against the SCA expansive pressure are given in Fig. 6. The left axis is the radial strain, and the bottom axis is the applied SCA

Table 1
Mechanical properties of the test equipment materials.

Material	Tensile Strength (MPa)	Yield Strength (MPa)	Elastic modulus (GPa)	Poisson's ratio	Density(g/cm^3)	Thermal conductivity λ (W/m·K)
7075 Aluminum alloy[a]	572.3	503.0	63.0	0.251	2.88[a]	196
301 Stainless steel[b]	520.0	205.0	200.0	0.305	7.93[b]	16

Notes: a: PRC National Standard GB/T3880.2–2012, Wrought aluminum and aluminum alloy plates, sheet and strips for general engineering-Part2: Mechanical properties, Standardization Administration of the People's Republic China. Beijing, (2012). b: PRC National Standard GB/T 1220–2007, stainless steel bars, Standardization Administration of the People's Republic China. Standards Press of China, Beijing, China (2007).

expansive pressure. The top and bottom parts of the right axis are the strain variation ratio of two adjacent monitoring points, and the slope values of different monitoring point location curves, respectively.

Fig. 6 shows that the radial strain at a given monitoring point location (point 1 to 10 in Fig. 4) changes linearly for a given applied SCA expansive pressure. The linear curve-fitting equations to the strain-expansive pressure curves at each location are given in Table 2. The slope change curves at different positions (point 1 to 10) indicate the SCA expansive pressure decreases as the radial distance from the center of the test cylinder increases and reaches a minimum close to the outer edge of the test cylinder.

The strain changes faster against the applied SCA expansive pressure and is more sensitive to lower applied SCA expansive pressures. The strain variation ratio of two adjacent monitoring points decreases gradually as the distance from the center of the test cylinder increases and reaches a minimum at 61.25 mm (point 6). In the actual measurement process, it is envisaged that the strain gauge will be difficult to attach practically at locations 1 and 10 (Fig. 4) because of limited space.

The formulas in Table 2 are the relationships between SCA expansion pressure P and radial strain ε_ρ. The formulas were established from numerical modeling results. In the numerical modeling process, the model input parameters were based on the materials used, namely the 7075 Aluminum Alloy and include material density, elastic modulus, and Poisson's ratio. The SCA properties were implicitly used in deciding on the model input pressures to simulate the SCA expansion. Hence, the formulas are material type and numerical modeling accuracy dependent. The authors note that for other materials different from what was used in this study, the process should be repeated to establish the equivalent equations in Table 2.

An expansive pressure calculation equation (Eq. (6)) developed by Gholinejad and Arshadnejad [30] is independent of the test system material (e.g. cement, aluminum, plastics, and steel) type. This equation can be used independent of the material type used in the test device for SCA expansive pressure test provided its Young's modulus is known. The equation provides a new insight for research on SCA expansive pressure testing and could be used as a guide in other studies in the future for material independent equations in analyzing test results.

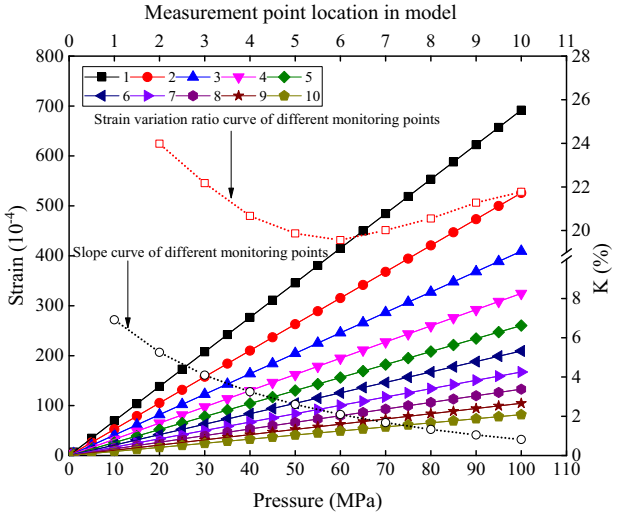

Fig. 6. Relation between strains and expansive pressures at different measurement point locations.

Table 2
Relation between the radial strains and the SCA expansive pressure at different measurement positions.

Strain monitoring point	Distance from the center of the test cylinder (mm)	Expansion pressure P vs radial strain ε_ρ (10^{-6} MPa)	Adj. R^2
1	42.5	$P = 6.918 \times \varepsilon_\rho + 0.012$	1
2	46.25	$P = 5.259 \times \varepsilon_\rho - 0.019$	1
3	50.0	$P = 4.093 \times \varepsilon_\rho + 0.008$	1
4	53.75	$P = 3.247 \times \varepsilon_\rho + 0.009$	1
5	57.5	$P = 2.602 \times \varepsilon_\rho - 0.008$	1
6	61.25	$P = 2.093 \times \varepsilon_\rho - 0.024$	1
7	65.0	$P = 1.674 \times \varepsilon_\rho + 0.035$	1
8	68.75	$P = 1.330 \times \varepsilon_\rho - 0.007$	1
9	72.5	$P = 1.047 \times \varepsilon_\rho - 0.005$	0.9999
10	76.25	$P = 0.819 \times \varepsilon_\rho + 0.018$	0.9999

4. Test equipment design and use in the upper end surface method

4.1. Test equipment

4.1.1. Equipment design

The test equipment in the UESM consists of a 2-section hollow thick-walled aluminum alloy cylinder, sealing platens, constraining connecting rods and strain gauges (Fig. 3).

The geometry of the UESM test equipment with strain measurements on the upper surface of the larger diameter section (Fig. 3) is similar to a press-fit system described by Perry and Aboudi [32], but with no interference (there is no interface between the internal diameters of the two cylinders and the material is the same aluminum alloy). The geometries of the two sections of the test cylinder are different. Following [33], based on cylinder length to thickness ratios in the proposed test equipment design, the upper cylinder falls in the plane strain domain while the lower section falls in the plane stress category. This type of problem can only be solved using 3D numerical modelling [33].

As explained earlier in Sections 3 and 7, in the case of the proposed UESM, the problem can only be modelled numerically to find the strain and expansion pressure relationships. In practice, strain gauges are attached diametrically orthogonal to the upper surface of the 150-mm diameter test cylinder top surface for strain measurements, as shown in Fig. 4.

The upper end surface of the proposed UESM test device platen has a central hole with a diameter of 5 mm so that the water vapor in the SCA reaction process can be discharged. This hole is also used later for injection of oil for the UESM calibration test described in Section 5.

To reduce the influence of heat released in the hydration reaction on the strain measurement and to have enough room for the attachment of strain gauges in the top surface of the lower 200-mm long 150-mm diameter section of the UESM test cylinder, the outer radius of this section of cylinder (b) should not be less than two times its inner radius (a) (i.e. $b \geq 2a$).

In the design of the proposed UESM test system the effect of temperature from the exothermal reaction of the SCA on the strain gauges to be used on the upper surface of the test cylinder is crucial. Consider a thick-walled hollow cylinder shown in Fig. 7 and assume the outer and inner surfaces are maintained at temperatures T_1 and T_2 respectively, with $T_1 < T_2$ and the elastic state of stress and constant physical properties are independent of the position and temperature [34]. Also assume that heat flows only in the radial direction with heat flow in the axial and circumferential directions being constant [34,35]. Based on these assumptions, the following boundary conditions apply.

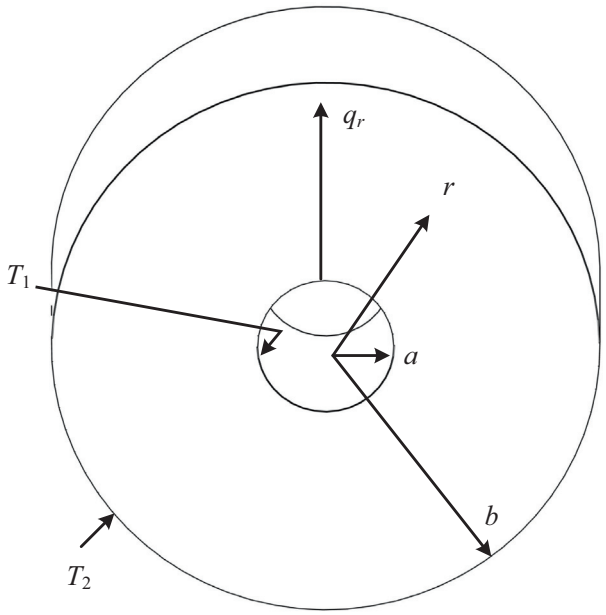

Fig. 7. Sketch for heat transfer calculation in a thick-walled cylinder.

Constant heat flow in axial (z) direction:

$$\frac{\partial T}{\partial Z} = 0 \tag{9}$$

Constant heat flow in tangential or circumferential direction:

$$\frac{\partial T}{\partial \phi} = 0 \tag{10}$$

Steady state:

$$\frac{\partial T}{\partial t} = 0 \tag{11}$$

Given that λ is the heat conductivity coefficient of the aluminum allow and q_r is the heat flux density we have [34,35].

$$\frac{\partial q_r}{\partial t} = -\frac{1}{r}\frac{\partial}{\partial t}(\lambda r \frac{\partial T}{\partial t}) \tag{12}$$

$$r\frac{\partial T}{\partial t} = C_1 \tag{13}$$

$$T = C_1 \ln r + C_2 \tag{14}$$

At $r = a$, $T = T_1$ and at $r = b$, $T = T_2$ and hence:

$$C_1 = \frac{T_1 - T_2}{\ln a - \ln b} = -\frac{\Delta T}{\ln \frac{b}{a}} \tag{15}$$

$$q_r = -\lambda \frac{dT}{dr} = -\lambda \frac{C_1}{r} = \lambda \frac{\Delta T}{r \ln \frac{b}{a}} \tag{16}$$

The temperature difference between the inside and outside of the thick-walled cylinder is calculated as in Eq. (17):

$$\Delta T = \frac{q_r \times r \times \ln \frac{b}{a}}{\lambda} \tag{17}$$

where ΔT is temperature difference (T_1-T_2); λ the thermal conductivity of the aluminum alloy; q_r the density of heat flux; a and b the inside and outer radii of the thick-walled cylinder.

From Eq. (17), the temperature difference between the inside and outside of a thick-walled cylinder is a function of the ratio of the outside radius (b) to the inside radius (a) and the thermal conductivity (λ) of the cylinder material. Therefore, the temperature difference ΔT cannot be determined by the thermal conductivity of the material (λ) alone, and the thickness of the cylinder wall must be considered. In Section 7, temperature monitoring results during SCA expansivity testing with the OPM and UESM are presented and discussed.

The hydration reaction of SCA (Eq. (18)) releases much heat and generates water vapor that evaporates, and hence, the test cylinder is not completely filled with the SCA slurry to allow for this additional fluid volume.

$$CaO + H_2O = Ca(OH)_2 + 64.8\ kJ \tag{18}$$

4.1.2. Test equipment material

Under a certain pressure condition, a stiffer metallic material has a smaller strain than a less stiff one, which can lead to large errors in pressure measurements in the former. A material undergoes a longer elastic stage if it has higher yield strength. The outer pipe method normally uses the 301 type stainless steel pipe for the measurement, while the proposed upper end surface method chooses the 7075 type aluminum alloy material to manufacture the test equipment. Compared with the 301 type stainless steel, the 7075 type aluminum alloy material has a smaller elastic modulus and higher yield strength as shown in Table 1 for the two types of materials.

4.1.3. Equipment machining

A solid aluminum alloy ingot with a diameter of 150 mm was machined by turn-milling to a diameter of 150 mm in the lower 200 mm of its height and 75 mm in the upper 50 mm of its height for a total height of 250 mm with surface smoothness tolerance of ± 0.05 mm. Using precision machining, a 50-mm diameter hole was bored through the center of the machined aluminum ingot. The fabricated UESM equipment including the datalogger as used in the testing is shown in Fig. 8.

4.2. Use of the upper end surface method equipment in SCA expansive pressure measurements

The SCA expansion pressure is measured by the upper end surface method in the following steps:

(1) Clean the test equipment. The oil and dust at the surfaces of the test equipment are cleaned with alcohol absorbent cotton.
(2) Mark the strain measurement points. In the numerical model, ten strain measurement points are marked along the radial direction from the center of the drilled hole in the test cylinder starting at the transition of the 75-mm diameter and 150-mm diameter interface of the test cylinder at equal distances from each other as shown in Fig. 4. In the actual experiments four strain gauges are attached diametrically orthogonal to the test cylinder as shown in Fig. 3.

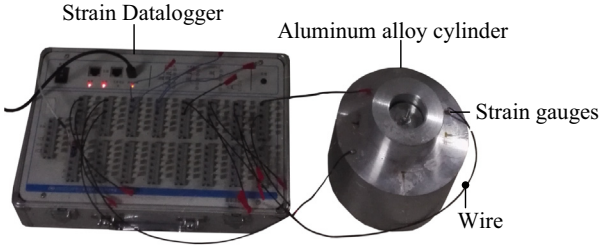

Fig. 8. UESM equipment as used in the test showing cylinder and strain datalogger.

(3) The strain gauges are glued to the marked diametrical diagonal measurement points.
(4) Strain gauge protection. After the strain gauges are firmly attached, a masking paper is taped around the wire connections of the strain gages at the upper end surface of the 150-mm diameter section of the test equipment to avoid electric conduction between the conducting wire and the upper end surface of the test equipment.
(5) The test equipment is placed on the lower sealing platen. The SCA is then poured into the test cylinder and the upper sealing platen is put in place, and the connecting rods fixed to the upper and lower sealing platens and tightened.
(6) A strain datalogger (Fig. 8) is connected to the conducting wires of the strain gauges to collect the strain data due to the expansion effect of the SCA.

The data collection is started immediately after the lower and upper end surface platens are tightened. Data collection is continued until the strains become constant, indicating SCA expansion has ceased or reached its limit, normally up to 24 h. Throughout the tests, the hole in the upper platen is left open to allow for release of the water vapor generated from the heat during the reaction of the SCA. This also makes the experiment identical to how it is applied in industrial settings for rock fragmentation.

5. Calibration of test equipment

5.1. Calibration equipment design

Fig. 9 shows details of the calibration equipment using oil pressure to simulate the SCA expansion pressure. Seal grooves (with rectangular cross-sections) were machined in the upper end surface of the top platen and the central part of the lower end surface platen. The seal groove has a width of 4.8 mm and depth of 2.74 mm. The O-ring with dimensions of 59.55 mm (in outer diameter) was used for the sealing process to prevent oil leakage. An oil injection connector is located at the center of the top sealing platen (cover plate) to inject 46# hydraulic oil at set pressures to simulate SCA expansion.

5.2. Experimental procedure

5.2.1. Accessory equipment

A servo-controlled loading system was used as the pressure supply source to the equipment. The oil outlet is connected to the oil inlet of the test equipment through a high-pressure hose. The 204-type bonded-foil gauge (resistance of 12 Ω) and the JM3812 type strain instrument were used.

5.2.2. Calibration procedure

Four measurement points were marked diametrically orthogonally at the top end surface of the 150-mm diameter section of the test cylinder as shown in Figs. 3 and 4. Four strain gauges were placed at the marked points to measure the radial strains in the SCA expansion process.

The equipment was filled with type 46 hydraulic oil, and the air in the equipment was bled. Then the end platens were tightly screwed-on. A high-pressure oil hose was connected to the oil inlet of the test equipment. The pressure at the oil source was adjusted to control the oil pressure level as required in the test cylinder. Once the experiment was completed, the switch at the oil source was shut off and the pressure released.

5.2.3. Calibration test schemes and results

In the calibration tests, the oil pressures were increased from 0 to 100 MPa at intervals of 5 MPa. Each pressure level was held for 5 min. The oil pressure at the oil pump and the strain values measured by the strain gauges were then recorded with a datalogger (Fig. 8). Each experimental scheme was repeated 4 times, and the average of the strain values was used for further analysis.

The pressure (P) was derived from the measured strains based on the equations in Table 2 that relate the applied pressures and strains at the measurement points from the numerical modeling. The equations in Table 2 were obtained by curve-fitting as explained earlier.

The percent difference E_r (Eq. (19)) between the calculated pressures P from equations in Table 2 and the known applied oil pressures P_0 were considered as the errors in the UESM.

$$E_r = \frac{P - P_0}{P_0} \times 100\% \tag{19}$$

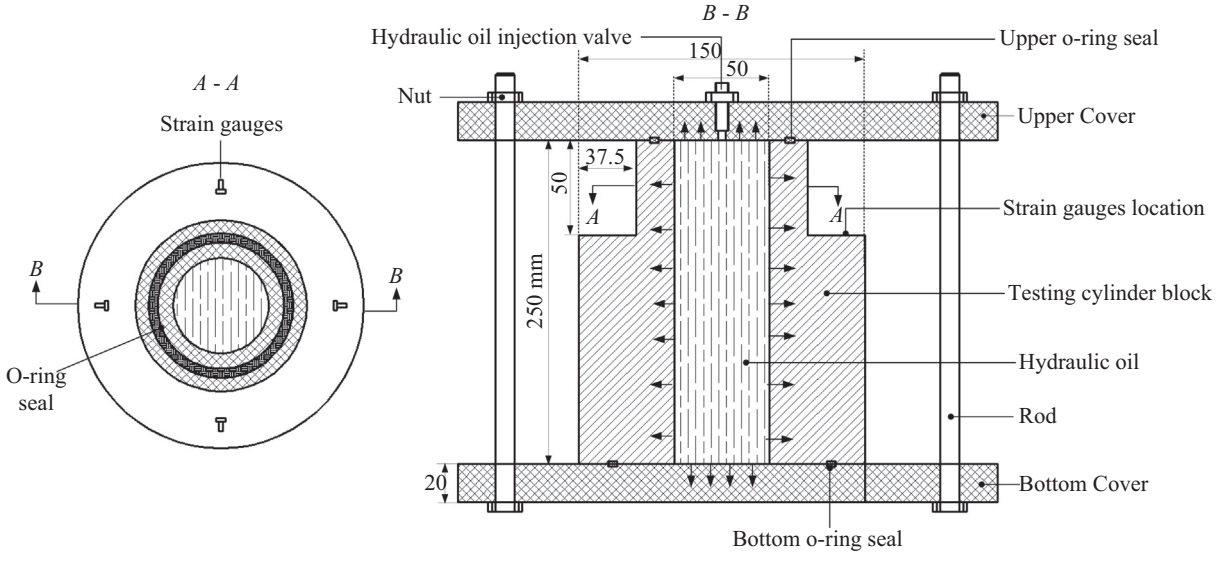

(a) Plan view showing oil sel ring (b) Section view of section *B-B*

Fig. 9. UESM calibration equipment test setup using oil pressure.

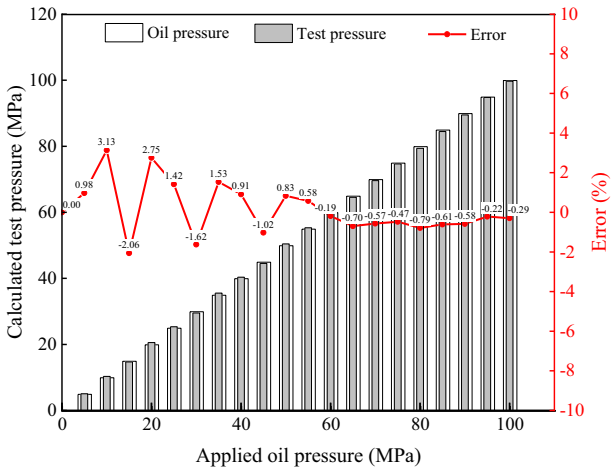

Fig. 10. The error of the oil pressure vs test pressure in UESM calibration.

The calibration test results are plotted in Fig. 10. As shown in the figure, the calculated pressures from the strains approximate the actual applied oil pressures, and the errors are less than 4%. The errors are higher at applied oil pressures less than 40 MPa. The oil pressure calibration results indicate that the measurement results obtained by the upper end surface method are consistent with the numerical simulation results. Therefore, the upper end surface method can be used to measure SCA expansive pressures reliably.

6. Expansive pressure measurement of SCA with the upper end surface method

6.1. Experimental schemes for the upper end surface method

The upper end surface method was used to measure the expansive pressure of SCA at different water contents (20%, 30% and 32%). The SCA used was that recommended by the China Building Materials Industry [36] and its composition was analyzed with X-Ray Diffraction (XRD) method and listed in Table 3.

SCA to water content percentages of 20%, 30% and 32% determined in terms of the mass of water to that of SCA were used for the following reasons: When the SCA-water percentage is less than 15%, the mixture appears as a wet clay and neither has the required viscosity to flow nor sufficient water for the hydration reaction (Fig. 11a). When the SCA-water ratio is greater than 32%, the viscosity of the slurry is too high and results in insufficient expansion pressure generation in a reasonable amount of time. For these reasons, most researches working on SCA limit themselves to SCA-water ratios in the range of 20–30%. This is also the water content range specified by SCA manufacturers and suppliers.

6.2. Preparation of SCA slurry and measurement of its expansive pressures

The SCA slurry was prepared in the following steps.

(1) Record the ambient room temperature (20 °C) and the water temperature (20 °C) were measured to determine the experiment environmental conditions as these are known to affect the expansivity of SCA in laboratory tests [27,37]. The SCA powder was mixed with the water at SCA powder to water ratios 1:5 (20%); 3:10 (30%) and 8:25 (32%). The SCA slurry was stirred for 5 min to ensure a consistent uniformly mixed slurry (Fig. 11b-11d).

(2) The SCA slurry was poured into the test equipment until it was full (Fig. 11f). The SCA slurry was then tamped down to bleed gas/air bubbles until the SCA slurry filled the inner hole of the test equipment.

(3) A thermometer was used to measure the temperatures at the strain measurement points on the upper end surface of the test equipment (Fig. 3). The measurement of the SCA expansive pressure was performed after the strain gauge readings were stabilized and balanced.

6.3. Analysis of experimental results

Fig. 12 provides a plot of the results for the SCA expansion at water contents of 20%, 30% and 32%. The SCA at a water content of 20% reacts for about 2.5 h, after which its expansive pressure reaches 10 MPa at 24 °C and retains this pressure for 5 h. The expansive pressure increased steadily as the reaction time increased. The expansive pressure tends to stabilize after 24 h, reaching a maximum value of 75 MPa in about 30 h. The maximum and minimum surface temperatures at the measurement positions were 24℃ and 22℃ respectively. The SCA at a water content of 30 % reacts after 2.5 h. The expansive pressure increased from 0 to 5 MPa and the reaction time changed from 2.5 h for the 20% water content to 5 h for the 30% water content. The expansive pressure increased continuously as the reaction time increased from 5 to 24 h and reaches a maximum of 42.5 MPa after 24 h. The maximum and minimum temperatures at the strain measurement positions were 22℃ and 19℃ respectively. The SCA at a water content of 32% reacted for 3 h. The expansive pressure increased to 2 MPa after a reaction time of 5 h, after which it increased gradually to a maximum of 35 MPa after 24 h. The maximum and minimum temperatures in the reaction process were 21℃ and 19℃ respectively. The results suggest that the temperature at the upper end surface changes slightly when the upper end surface method is used for the SCA expansive pressure measurement. Though the hydration process increased the temperature at the upper end surface, the temperature increment is relatively small and has limited influence on the strain gauge performance.

SCA exothermal reaction can generate temperatures of up to 150 °C [38]. These authors showed that low temperatures slow the hydration process and therefore SCA expansivity. For the same water content of SCA mixture, SCA expansive pressure increases with temperature [39] in the ambient temperature range of 20–45 °C [2,22]. This temperature range can still be accommodated by most standard strain gauges as they have temperature performance ranges in the range of 40–80 °C.

Fig. 12 shows that the initial SCA reaction temperature depends on the water content which is vital for the expansive pressure of the SCA. The smaller the water content the higher the SCA reaction temperature and potential expansive pressures. While Fig. 12 appears to suggest that smaller water contents will generate higher SCA expansive pressures. However, according to the literature, when the water cement ratio is between 20 and 30%, the amount of water fully meets the SCA hydration reaction needs. In this water content range, the viscosity of SCA slurry works best. When the water to SCA percentage is less than 20%, the viscosity of SCA slurry is extremely low to enable its application in boreholes and for complete exothermal reaction, and thus results in under expansivity and rock fragmentation for example. Based on Fig. 12 and Fig. 13, it appears there is a minimum water to SCA ratio (about 20%) for acceptable expansivity of SCA to perform its intended function. This also appears to be the optimum moisture content as below this level, insufficient water is available to support complete reaction, and allow sufficient viscosity for the product application. Water contents above this ratio delays the reaction and results in low expansive pressures.

Table 3
X-Ray Diffraction (XRD) quantitative component analysis results of the composition of the China Building Materials Industry (2008) SCA [36].

CaO (%)	Al_2O_3 (%)	MgO (%)	Retarding agent (%)	Water reducing agent (%)	Other (%)
85.0	3.0	3.0	3.0	2.0	4.0

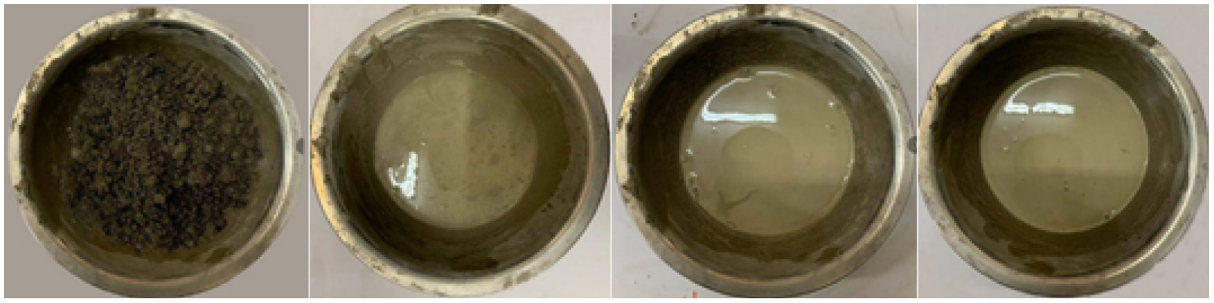

(a) 15% (b) 20% (c) 30% (d) 40%

(e) SCA slurry (f) SCA slurry poured into the test equipment

Fig. 11. The state of different SCA-water ratio mixtures.

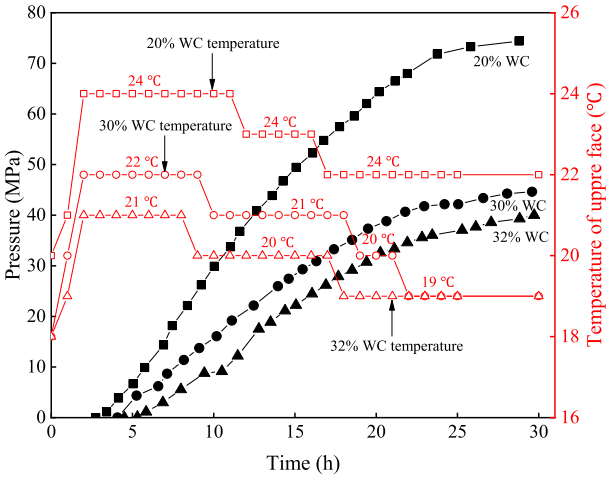

Fig. 12. SCA Expansive pressure measurement results at different water contents.

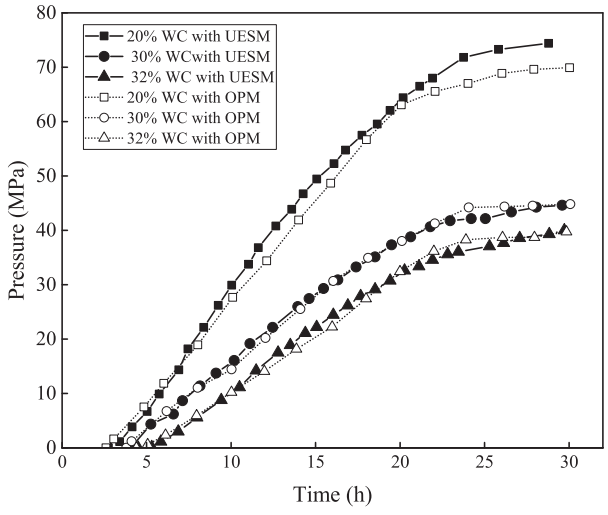

Fig. 13. SCA expansive pressure measurement results: comparison of OPM and UESM at different water contents.

Fig. 13 compares test results from the UESM and OPM using the same SCA product in the same environment. This comparison was necessary to show the reliability of the proposed UESM compared to the established OPM. The results of the two methods compare favorably and suggests that the proposed UESM can be used to study the expansivity of SCAs.

7. Discussion

7.1. Comparison between measurement results of the upper end surface and the outer pipe methods

The measurement results of the SCA expansive pressure using both the OPM and UESM in the same experimental conditions are given in Fig. 13. The authors hypothesized that the reliability of the results of the two methods largely depends on the two different types of materials used in the construction of the two test systems. A 301-type stainless steel pipe is used in the outer pipe method (OPM) while a type 7075 aluminum alloy material is used in UESM. The properties of the two types of materials are provided in Table 1 for comparison. Additionally, in the OPM, the inner radius of the stainless-steel test pipe is 25 mm with a wall thickness ($(b\text{-}a)_{opm}$) of 1.5 mm for an external radius of 26.5 mm. In the USEM case, the test cylinder consists of two sections, a 50-mm long 25-mm-internal radius section with a wall thickness ($(b\text{-}a)_{uesm}$) of 12.5 mm for an external radius of 37.5 mm and 200 mm long 25-mm internal radius section with a wall thickness of 50 mm for an external radius of 75 mm. In the UESM test, the measurements are taken on the top surface of the 50-mm thick section of the 2-section test cylinder.

According to Hertzberg et al. [40] pressure vessels are thick-walled cylinders when wall thickness (b-a) to internal radius (a) ratio is less than or equal 0.1 ($(b\text{-}a)/a \leq 0.1$). Hence, for the given test cylinders dimensions, both UESM and OPM satisfy the criterion for thick-walled cylinders with the difference that the cylinder thickness in UESM is 31.25 times that of the OPM test cylinder thickness. This has implications on the temperature of the outer cylinder in the tests as can be seen in Eq. (17).

During the SCA expansivity testing with the OPM and UESM for comparison the temperatures of the outer walls of the two test methods cylinders were monitored. The temperature monitoring results of the two tests are shown in Fig. 14. In Fig. 14, at the initial stage of the SCA hydration reaction, the outer surface temperature of the 7075 Aluminum Alloy for the UESM is faster than that of the outer surface temperature of the 301 stainless steel pipe in the OPM. This is mainly because heat flux density (q_r) in Eq. (17) and the thermal conductivity (λ) of the 7075 Aluminum Alloy are higher. When the SCA hydration reaction time t = 3 h, the surface temperature of 7075 aluminum alloy reaches the highest value of 35℃, while the surface temperature of the 301 stainless steel tube reaches the highest value of 103℃ at the hydration reaction time t = 5 h. From the test results, the thermal conductivity of 7075 aluminum alloy in UESM is higher than that of 301 stainless steel pipe in OPM, and the surface temperature is lower than that of 301 the stainless-steel pipe in OPM.

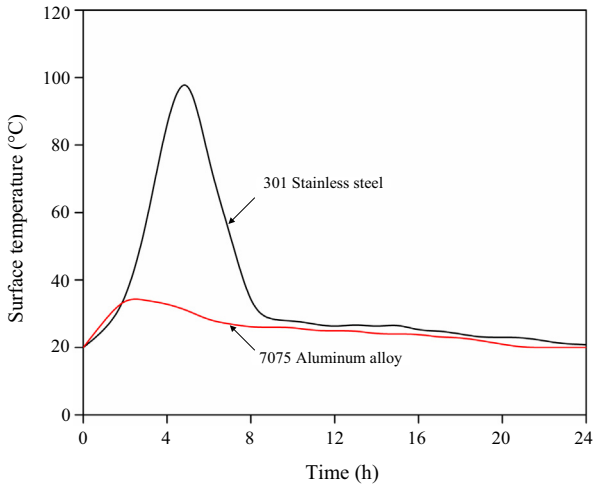

Fig. 14. Temperature monitoring results of at the outer test cylinder surface of the OPM and at r = 57.5 mm of the UESM tests in the same test environment.

Based on Eq. (17), the test cylinder characteristics of the two methods and Table 1, the temperature difference (ΔT) between the internal and external boundaries for OPM and UESM are 0.096507879 q_r and 0.24434834 q_r respectively. Note that in the case of the UESM the temperature difference of 0.24434834 q_r at a radius of 57.5 mm. This temperature difference for UESM could be increased to 0.36772122 q_r if measured at a radius of 70 mm which is permissible and possible. Since the thermal diffusivity (q_r) for 301 stainless steel is less than that for 7075 Aluminum Alloy [41], ΔT for 7075 aluminum alloy is higher than that for 301 Stainless steel. The significance of higher temperature difference is that SCA reaction temperature which can reach up to 150 °C at $r = a$ in both tests will be significantly lower at $r \geq 57.5$ mm in the UESM and justifies the use of this approach compared to the OPM approach.

The measurement results with the OPM in Fig. 13 show that the expansive pressure of the SCA at the three different water contents increased slowly with increasing reaction time, and almost became constant after 24 h. The expansive pressure magnitudes of the SCA at the water contents of 20%, 30% and 32% after 24-hour reaction time were 68, 44 and 39 MPa respectively. By comparing the measurement results of the final expansive pressure of the SCA by the OPM and the UESM at the three different water contents of 20%, 30% and 32%, the results differ by 6.4%, 0.4% and 0.7% respectively, with the highest difference occurring at the lowest water content of 20% at which the SCA expansive pressures are highest in the two methods. The small differences in the results between the OPM and UESM show that the UESM and OPM results are almost consistent and that the UESM can be used in SCA expansive pressure assessments instead of the OPM for both economic and user friendliness reasons, as stipulated earlier.

From the practical point of view, the measurement position of OPM is the outer pipe wall surface, which is curved. During the strain measurement, the surface curvature results in an error in the measurement. On the upper end surface is in the proposed UESM is flat. When strain gauges are used to measure deformation, the flatness of the measurement surface reduces the measurement error caused by surface curvature. Therefore, from the measurement location point of view, UESM is superior to OPM.

Additionally, the SCA produces a large amount of heat during the hydration reaction. The external surface temperature of the measuring device can reach 140–150 °C. Normal strain gauges working temperature is 40–80 °C. Therefore, when measuring strains with OPM, it is necessary to replace regular strain gauges with high-temperature strain gauges which are expensive or to submerge the testing system in ice-water mixture, and the bonding process to the pipe is also complicated. When measuring expansion pressure with the UESM, the temperature of the upper surface does not generally exceed the working temperature range of standard strain gauges due to the large wall thickness of the test cylinder and the thermal conductivity of the 7075 Aluminum Alloy, and the normal strain gauges with temperature compensation can be used. Therefore, from the perspective of measurement cost and measurement simplicity, UESM is superior to OPM.

7.2. Sensitivity of the OPM and UESM test cylinder materials: 301 stainless steel and 7075 aluminum alloy

7.2.1. Sensitivity in SCA expansive pressure measurement with the outer pipe method

In Section 1.2.2, Eq. (1) was given as the theoretical basis of OPM. By substituting the 301-type stainless steel material parameters into Eq. (1), Eq. (20) was obtained for calculation of the expansive pressure measured in the outer pipe method.

$$P_r = 289.45 \times \varepsilon_\theta + 72.65 \times \varepsilon_z \quad (20)$$

Eq. (1) shows that the sensitivity of the measured SCA pressure will depend on the type of material used to make the test cylinder; and Eq. (20) means this pressure will depend on the measured strains which are dependent on the sensitivity of the test cylinder material to strain changes.

The axial strain ε_z and the tangential strain ε_θ are required in Eq. (1) for the calculation of the expansive pressure. The outer pipe method measures the strain at the outer curved surface of the pipe. The curvature of the pipe surface influences the measurement accuracy. The pipe used in the outer pipe method has relatively small wall thickness ($(b\text{-}a)_{opm}$) of 1.5 mm. The heat released in the SCA hydration process increases the temperature at the strain measurement position to about 100 °C as shown Fig. 14. This exceeds the operating range of the standard strain gauges and influences their measurement accuracy. The practical solution is to always put the steel pipe into a cryostat or to use a strain gauge that is resistant to high temperatures. These remedies complicate the testing procedure and increases the testing cost.

7.2.2. Sensitivity in SCA expansive pressure measurement with the upper end surface method

The plane stress or plane strain assumption is not explicitly applicable to the upper end surface method due to the 2-section cylinder geometry. The internal pressure and the strain on the upper end surface of the 150-mm diameter section of the test cylinder is beyond the basic theory of plane strain or plane stress problems in elastic mechanics. Hence, numerical modelling was needed to establish the mathematical model relating the test cylinder internal pressure and the strain at the measurement position due to the SCA expansion. For example, the expansive pressure and the radial strain at the measurement position 5 (for r = 57.5 mm from the center of the 75-mm outer radius section of the test cylinder) in this paper satisfies Eq. (21). Note that r could be conveniently increased from 57.5 to 70 mm while allowing for the cylinder boundary constraints and enough room for installation of strain gauges to further lower the temperature at the outer boundary of the test cylinder in the UESM as explained in Eq. (17) in Section 4.

$$P = 2.602 \times \varepsilon_\rho - 0.008 \ (R^2 = 1) \quad (21)$$

In Eq. (21) only the radial strain ε_ρ is required for the calculation of the expansive pressure. The reliability of Eq. (21) depends on the accuracy of the numerical model and input parameters. Therefore, it is necessary to always establish an elaborate numerical model and to determine accurate input material parameters for use in the numerical model. Equally important is the precision and accuracy of the upper end surface and the accuracy of the strain gauges used. Finally, the accuracy of the expansive pressure measurement can be improved by a reasonable selection of the strain measurement positions and the strict implementation of the testing procedure.

7.3. Potential impact of using aluminum alloy instead of rock on results

Using either the type 301 stainless steel or the proposed 7075 aluminum alloy as materials for the SCA test cylinders in the OPM and UESM respectively instead of rock or concrete in which the SCA is often used, makes both methods indirect methods for the study of SCA expansivity. In Section 6.2.1, and Section 7.1, the difference in the results between the materials used in the UESM and OPM methods was discussed. Eq. (1) showed that the sensitivity of the measured SCA expansion pressure depends on the type of material used to make the test cylinder, and Eqs. (20) and (21) showed this pressure will depend on the measured strains which are dependent on the sensitivity of the test cylinder material to deform.

Both the 7075 Aluminum alloy and 301 Stainless Steel used in the UESM and OPM respectively for the study of the expansivity of SCA differ from rock and concrete in which the SCA is often used. Rock and concrete are relatively more porous compared to the 7075 Aluminum Alloy and 301 Stainless Steel used to make the test cylinders for the SCA expansivity studies. The rock and concrete are also less heat conductors compared to the aluminum alloy and stainless steel used. Therefore, in rock more of the heat generated from the exothermal reaction, which can result in temperatures of up to 150 °C [38] will be retained. These authors [38] showed that low ambient temperatures slow the SCA hydration process and therefore SCA expansivity. For the same water content of SCA mixture, SCA expansive pressure increases with temperature [39] in the ambient temperature range of 20 °C to 45 °C [2,25]. The SCA hydration process is more efficient in the manufacturers specified temperature range and water contents. Thus, as stated in [5], because the thermal properties of the steel and aluminum alloy cylinders and rock are substantially different, and since the expansive pressure is a function of the thermodynamics, SCA expansive pressure development may vary in the three systems.

Rocks in petroleum and mining engineering are porous media. In petroleum engineering drilling and well completion fluids are required that are expensive. Loss of these drilling and well completion fluids in the porous reservoir rocks is economically costly to oil production [42,43]. One approach to managing fluid loss in porous media is to use fluid loss additives which include calcium oxide (i.e. SCA). Fluid loss additives plug rock pores to prevent fluid loss. Thus, in relating the test results to actual field applications in rock with relatively higher porosity one would not expect major deviations as the SCA to some extent might plug the rock pores to reduce loss of water through diffusion. Further research is required in this area.

In practice, when SCA is used in rock or concrete part of the water in the slurry will infiltrate or diffuse into the voids, resulting in the change of SCA to water ratio and lead to a faster reaction rate and time of the SCA slurry [44-49]. As a result of this, the higher SCA output swell pressure could result in rock and concrete than in the metallic test cylinders, provided sufficient water is present to enable complete chemical reaction [47]. In principle, lower SCA to water ratios result in higher SCA expansive pressures as demonstrated in Fig. 13.

Because of the relatively impervious nature of the 7075 Aluminum Alloy in the UESM compared to rock, SCA expansion pressure will be less in UESM for equal SCA to water ratios. This is because water diffusivity in rock will result in lower SCA to water ratio and thereby result in a possible accelerated chemical reaction and more expansivity. UESM test cylinder will not lose water through diffusion, and the hydration process will be slower compared to rock. Therefore, whether the 7075 Aluminum alloy material of UESM or the 301 Stainless Steel material of OPM is used in the SCA expansivity studies, neither can fully simulate the change

in the SCA to water ratio caused by the diffusion of water in actual SCA application.

8. Conclusions

The numerical calculation results of the SCA expansive pressure measurement process with the upper end surface method indicates that the expansive pressure changes linearly with the radial strain at the upper end surface of the 150-mm diameter section of the test cylinder used. The mathematical model relating the expansive pressure and the radial strain was established based on numerical simulation. The SCA expansive pressure in the test equipment can be calculated using the measured radial strain data. The equation developed (Eq. (21)) is dependent on the UESM test cylinder material properties and the accuracy of the numerical model.

Because the UESM test cylinder thickness and material diffusivity are far greater than those of the OPM, the temperature at the outer surface of the UESM test cylinder is far less than in the OPM, and therefore suits the use of standard strain gauges and eliminates the use of coolants such as submerging the test system in water with ice, and special high temperature strain gauges or cryostat that is required in the OPM.

The oil pressure calibration results are consistent with the measurement results of the upper end surface method. This indicates that the expansive pressure calculation equation established with the numerical simulation of the upper end surface method is reliable and is applicable for the measurement of the SCA expansive pressure.

The measurement results of the SCA expansion pressures at the same water contents and under similar experimental conditions with the upper end surface and outer pipe methods are consistent with each other. This further proves the feasibility and accuracy of the upper end surface method.

The measurement principle, measurement process and the material type used in the OPM complicates the method and makes its use unfriendly and costly. The relation between the pipe wall thickness and the pipe wall temperature due to the SCA material reaction is the main source of problem in the outer pipe method.

The upper end surface method eliminates the problems encountered in the outer pipe method, simplifies the testing procedure, reduces the cost of testing, and improves the measurement accuracy.

The UESM and OPM approaches are indirect methods for studying SCA expansive pressure since the test cylinder materials in both tests are different from rock and concrete in which the SCA is used.

Future studies will establish SCA expansive pressure measurement equations for the UESM that are independent of the test cylinder material type.

Declaration of Competing Interest

The authors declare that they have no known competing financial interests or personal relationships that could have appeared to influence the work reported in this paper.

Acknowledgements

This study was funded by the State Key Research Development Program of China (No. 2018YFC0604400), the National Science Foundation of China (Nos. 51874068, 52074062), the Fundamental Research Funds for the Central Universities (Nos. N2001003, N160107001, N180701016, N182608003, N2001001), and the 111 Project (No. B17009). The authors also acknowledge Nazarbayev University for funding the research through its Collaborative Research Program (No. OPCRP2020014).

References

[1] Wang Y, You B, Zhang G. Application of soundless cracking agent in china. Demolition and Reuse of Concrete and Masonry. Abingdon, UK: Chemical Rubber Company Press; 1988.
[2] Hinze J, Brown J. Properties of soundless chemical demolition agents. Journal of Construction Engineering and Management 1994;120(4):816–27.
[3] Akhvlediani T, Mataradze E, Chikhradze N, Gabadadze T, Suladze I. Investigation of new non-explosive demolition agent for use at underground mining of hard ores. International Multidisciplinary Scientific Geo Conference: SGEM 2008;1(1):281.
[4] Étkin M, Azarkovich A. Effect of non-explosive splitting compounds and rational work parameters. Power Technology and Engineering 2006;40 (5):287–92.
[5] Dowding CH, Labuz JF. Fracturing of rock with expansive cement. Journal of the Geotechnical Engineering Division 1982;108(10):1288–99.
[6] Shang J, Zhao Z, Aliyu MM. Stresses induced by a demolition agent in non-explosive rock fracturing. Int J Rock Mech Min Sci 2018;107:172–80.
[7] Harada T, Soeda K, Idemitsu T, Watanabe A. Characteristics of expansive pressure of an expansive demolition agent and the development of new pressure transducers. Doboku Gakkai Ronbunshu 1993;1993(478):91–100.
[8] De Silva VRS, Ranjith PG, Perera MSA, Wu B, Rathnaweera TD. The influence of admixtures on the hydration process of soundless cracking demolition agents (SCDA) for fragmentation of saturated deep geological reservoir rock formations. Rock Mech Rock Eng 2019;52(2):435–54.
[9] Zhai C, Xu J, Liu S, Qin L. Fracturing mechanism of coal-like rock specimens under the effect of non-explosive expansion. Int J Rock Mech Min Sci 2018;103:145–54.
[10] Hao B, Hu S, Cheng J, Huang H, Kang KWL. Mechanism analysis of rock breaking using static cracking agent (SAC). Electron J Geotech Eng 2014;19:Z6.
[11] Gambatese JA. Controlled concrete demolition using expansive cracking agents. Journal of Construction Engineering and Management 2003;129 (1):98–104.
[12] Xu S, Hou P, Li R, Cai M. An experimental study on the mechanical properties and expansion characteristics of a novel self-swelling cartridge for rock breakage. Rock Mech Rock Eng 2021;54(2):819–32.
[13] Guo T, Zhang S, Ge H, Wang X, Lei X, Xiao Bo. A new method for evaluation of fracture network formation capacity of rock. Fuel 2015;140:778–87.
[14] Guo T, Zhang S, Ge H, Qu Z. A novel "soundless cracking agent fracturing" for shale gas reservoir stimulation. International Journal of Environmental Science and Development 2015;6(9):681–7.
[15] De Silva VRS, Ranjith PG, Perera MSA, Wu B, Wanniarachchi WAM. A low energy rock fragmentation technique for in-situ leaching. J Cleaner Prod 2018;204:586–606.
[16] Xu S, Hou P, Cai M, Li Y. An experiment study on a novel self-swelling anchorage bolt. Rock Mech Rock Eng 2019;52(11):4855–62.
[17] Xu S, Yang Z, Cai M, Hou P. An experimental study on the anchoring characteristics of an innovative self-swelling Split-set. Tunn Undergr Space Technol 2021;112:103919. https://doi.org/10.1016/j.tust.2021.103919.
[18] Ramachandran VS, Sereda PJ, Feldman R. Mechanism of hydration of calcium oxide. Nature 1964;201(4916):288–9.
[19] Goto K, Kojima K, Watabe K. The mechanism of expansive pressure and blow-out of static demolition agent. In: Conference of Demolition and Reuse of Concrete and Masonry. Nihon University; 1988.
[20] Swanson D, Labuz J. Behavior of a calcium oxide-based expansive cement. Concr Sci Eng 1999;1(3):166–72.
[21] Harada T, Idemitsu T, Watanabe A, Takayama S-i. The design method for the demolition of concrete with expansive demolition agents. In: Fracture of Concrete and Rock. Berlin, Germany: Springer; 1989.
[22] De Silva VRS, Ranjith PG, Perera MSA, Wu B, Rathnaweera TD. Investigation of the mechanical, microstructural and mineralogical morphology of soundless cracking demolition agents during the hydration process. Mater Charact 2017;130:9–24.
[23] Tang L, Tang C, Tang S, Cui Y, Song L. Physical experiment and numerical simulation on effect of soundless cracking agent. Chinese Jounal of Geotechnical Engineering 2005;27(4):70–4. in Chinese.
[24] Laefer DF, Ambrozevitch-Cooper N, Huynh MP, Midgette J, Ceribasi S, Wortman J. Expansive fracture agent behaviour for concrete cracking. Mag Concr Res 2010;62(6):443–52.
[25] Natanzi AS, Laefer DF, Connolly L. Cold and moderate ambient temperatures effects on expansive pressure development in soundless chemical demolition agents. Constr Build Mater 2016;110:117–27.
[26] De Silva VRS, Ranjith PG, Perera MSA, Wu B, Rathnaweera TD. A modified, hydrophobic soundless cracking demolition agent for non-explosive demolition and fracturing applications. Process Saf Environ Prot 2018;119:1–13.
[27] Laefer DF, Natanzi AS, Zolanvari SMI. Impact of thermal transfer on hydration heat of a Soundless Chemical Demolition Agent. Constr Build Mater 2018;187:348–59.
[28] Popov E, Nagarajan S, Lu Z. Mechanics of materials. London: Prentice Hall; 1978.

[29] Timoshenko S, Goodier J. Theory of Elasticity. New York: McGraw-Hill Book Company Inc; 1951.
[30] Gholinejad M, Arshadnejad S. An experimental approach to determine the hole-pressure under expansion load. J South Afr Inst Min Metall 2012;112(7):631–5.
[31] Itasca. Flac3D software. Minneapolis, US: Itasca Consulting Ltd; 2019.
[32] Perry J, Aboudi J. Elasto-plastic stresses in thick walled cylinders. J. Pressure Vessel Technol. 2003;125(3):248–52.
[33] Kamal SM, Dixit US, Roy A, Liu Q, Silberschmidt VV. Comparison of plane-stress, generalized-plane-strain and 3D FEM elastic–plastic analyses of thick-walled cylinders subjected to radial thermal gradient. Int J Mech Sci 2017;131-132:744–52.
[34] Dzierwa P, Taler D, Taler J. Optimum heating of cylindrical pressure vesselsOptimierte Erwärmung zylindrischer Druckbehälter. Forsch Ingenieurwes 2015;79(3-4):163–73.
[35] Serth RW, Lestina T. Process heat transfer: Principles, applications and rules of thumb. Pittsburgh, US: Academic press; 2014.
[36] China NDaRC, Soundless cracking agent. Beijing: Building Materials Industry Press; 2008.
[37] Natanzi AS, Laefer DF, Kakali G, Iman Zolanvari SM. Temperature-induced chemical changes in soundless chemical demolition agents. J Mater Civ Eng 2019;31(7):04019098. https://doi.org/10.1061/(ASCE)MT.1943-5533.0002653.
[38] Huynh MP, Laefer DF, McGuill J, White A. Temperature-related performance factors for chemical demolition agents. International Journal of Masonry Research and Innovation 2017;2(2–3):220–40.
[39] Soeda K, Harada T. The mechanics of expansive pressure generation using expansive demolition agent. Doboku Gakkai Ronbunshu 1993;1993(466):89–96.
[40] Hertzberg RW, Vinci RP, Hertzberg JL. Deformation and fracture mechanics of engineering materials. US: John Wiley & Sons; 2020.
[41] Ashby MF. Materials and the Environment (2nd Edition). Oxford, England: Butterworth-Heinemann; 1992.
[42] Johannes K. Petroleum engineer's guide to oil field chemicals and fluids. Oxford: Gulf Professional Publishing; 2012.
[43] Xu S, Liang R, Suorineni FT, Li Y. Evaluation of the use of sublevel open stoping in the mining of moderately dipping medium-thick orebodies. International Journal of Mining Science and Technology 2021;31(2):333–46.
[44] Tang W, Zhai C, Xu J, Sun Y, Cong Y, Zheng Y. The influence of borehole arrangement of soundless cracking demolition agents (SCDAs) on weakening the hard rock. International Journal of Mining Science and Technology 2021;31(2):197–207.
[45] Vennes I, Mitri H, Chinnasane DR, Yao M. Large-scale destress blasting for seismicity control in hard rock mines: A case study. International Journal of Mining Science and Technology 2020;30(2):141–9.
[46] Jing H, Wu J, Yin Q, Wang Ke. Deformation and failure characteristics of anchorage structure of surrounding rock in deep roadway. International Journal of Mining Science and Technology 2020;30(5):593–604.
[47] Li L, Ma C, Hu S, He M, Yu H, Wang Q, et al. Effect of the benzene ring of the dispersant on the rheological characteristics of coal-water slurry: Experiments and theoretical calculations. International Journal of Mining Science and Technology 2021;31(3):515–21.